Scanning Microscopy Supplement 1, 1987 (Pages 229-240)
Scanning Microscopy International, Chicago (AMF O'Hare), IL 60666 USA

SCANNING ELECTRON MICROSCOPY WITH POLARIZATION ANALYSIS: HIGH RESOLUTION IMAGES OF MAGNETIC MICROSTRUCTURE

G.G. Hembree, J. Unguris, R.J. Celotta, D.T. Pierce*

National Bureau of Standards
Gaithersburg, MD 20899, USA

Abstract

Secondary electrons from a ferromagnet exhibit a spin polarization related to the net spin density of the valence electrons, i.e., directly proportional to the magnetization. Thus, secondary electron polarization analysis provides a direct measurement of the magnitude and direction of the magnetization in the area probed by the incident electron beam in the Scanning Electron Microscope (SEM). The polarization measurement is independent of topographic contrast and is obtained simultaneously with the conventional topographic image. A new, compact (approximately fist-sized), polarization analyzer utilizing low energy (150 eV) diffuse scattering from a polycrystalline Au target was specially developed for this application. The small size of the spin analyzer allowed the use of two orthogonal analyzers on a field emission SEM to detect all three components of the magnetization vector. Images from Fe-3%Si demonstrate the independence of magnetic and topographical contrast except in special cases where the topography affects the magnetism, e.g., by pinning domain walls. Practical application of Scanning Electron Microscopy with Polarization Analysis (SEMPA) to study closure domains in permalloy thin film recording heads and to observe the magnetic microstructure of a CoNi thin film recording high density media will be discussed. The variation of the spin within a domain wall of an Fe-based ferromagnetic glass is observed.

Key Words: Magnetic microstructure, scanning electron microscopy, domain imaging, electron spin polarization images, secondary electron polarization, spin polarization analysis.

*Address for Correspondence:
D.T. Pierce
National Bureau of Standards
Bldg. 220, Room B206
Gaithersburg, MD 20899
Phone no.: (301) 975-3711

Introduction

Efforts to observe magnetic microstructure span half a century. A knowledge of the magnetic microstructure includes the shape and size of domains, the direction of magnetization in each domain, and how the magnetization changes within a domain wall. All of this information is available if the magnetization vector $\vec{M}(\vec{r})$ is known at each point of a sample. The terms of the Hamiltonian for a ferromagnetic system that give rise to domains can be listed but the microscopic magnetic structure still cannot be calculated. Yet, magnetic microstructure is becoming increasingly important. A major emphasis of magnetic technology is increased density of information storage which means smaller domain sizes and reduced dimensions of magnetically active elements in devices such as read/write heads. Also, the influence of size effects and dimensionality, such as the presence of a surface, on domain wall formation and movement poses some fundamental physical questions for exploration. There is a clear need to determine magnetic microstructure with increased spatial resolution (Celotta and Pierce, 1986). At present there are several techniques to observe magnetic microstructure, each with certain strengths as well as limitations.

The oldest and simplest method for domain observations is the Bitter (1931) magnetic powder pattern technique wherein magnetic colloidal particles collect in stray field gradients at domain walls. The requisite stray fields may be weak in high permeability materials and in any case are only indirectly related to the magnetization. The powder patterns are generally viewed with an optical microscope which limits the resolution to approximately one micrometer.

Magneto-optic effects for domain observation, known as the Faraday effect in optical transmission and Kerr effect on reflection, have the advantage that the rotation of the light polarization vector is directly related to the magnetization. In addition, dynamic measurements are possible and large magnetic fields may be applied. On the other hand the technique is limited to optical resolution, the contrast is low, and images are subject to interference from sample topography.

The highest resolution domain images are obtained by transmission electron microscopy (TEM). The conventional technique in the TEM is Lorentz microscopy (Jakubovics, 1973) wherein the deflection

of the electron beam as it passes through the magnetic field in the specimen produces contrast which can be observed in the defocussed image. Higher resolution is achieved by two new techniques, electron holography (Tonomura, 1983) and differential phase contrast microscopy (Chapman and Morrison, 1983). Specimens must be sufficiently thin for transmission techniques (usually $\lesssim$100 nm) which can be a disadvantage since the very nature of the magnetic structure--Bloch vs. Neel walls for example--depends sensitively on the thickness. The magnetic contrast is proportional only to the value of the in-plane component of the magnetic induction $\vec{B}$ averaged over the thickness of the specimen. Furthermore, the electron microscope image contains both magnetic and topographic contrast which may be difficult to separate.

For many applications it would be desirable to image magnetic domains of a thick specimen or to image magnetic structures on a nonmagnetic substrate, such as a bit written on a magnetic disk or a permalloy memory element on a silicon chip. This can be achieved in the SEM where, until recently, only two contrast mechanisms were possible (Newbury et al. 1986). In Type I contrast, the secondary electron image is affected by the stray fields outside the surface of the sample. In Type II contrast, the backscattered electron intensity is enhanced or decreased by the electron deflection in the in-plane magnetic induction $\vec{B}$ which changes from one domain to the next. Both of these techniques suffer from low contrast, limited resolution (of order 1 μm) and interference from surface topography. A new technique which overcomes each of these disadvantages and offers further advantages has been developed, and is the subject of this paper.

The new technique, scanning electron microscopy with polarization analysis (SEMPA), uses the highly focused unpolarized electron beam in a SEM to generate secondary electrons, the polarization of which is subsequently measured to obtain the magnetic information. The fact that secondary electrons emitted from a ferromagnet are spin polarized was discovered by Chrobok and Hofmann (1976). Because these first measurements lacked energy resolution (secondaries were collected over a 500 eV range), were performed in a high magnetic field (unlike the situation in an SEM where the secondaries make a transition to a field free region at the specimen surface), and because the uncertain composition of the EuO thin films prevented relating the polarization to material magnetic properties, the results of subsequent measurements were relied upon to further establish the basis for SEMPA. Unguris et al. (1982) made the first measurements of the energy distribution of the spin polarization of secondary electrons from a ferromagnetic glass $Fe_{81.5}$ $B_{14.5}$ Si_4, and found the polarization to be high at the peak of the secondary electron intensity and even higher at the lowest energies. Similar results were obtained from single crystal faces of Fe, Co, Ni (Kisker, et al., 1982; Hopster et al., 1983) which verified that the secondary electron spin polarization represents the net spin density of the valence electrons.

Some of the methods that have been considered for using electron spin polarization to produce magnetic contrast in SEM are; 1) a measurement of the asymmetry in the scattering of a spin polarization modulated polarized incident beam, 2) a measurement of the induced spin polarization when an unpolarized electron beam is elastically scattered from a ferromagnet, and 3) the measurement of the spin polarization of low energy secondary electrons (Celotta and Pierce, 1982; Kirschner, 1984). Of the three alternatives, the last is most easily adapted to current SEM technology. DiStefano (1978 and private communication) described the potential of combining electron spin polarization analysis and SEM to observe submicron sized magnetic bubbles. The following advantages of measuring the spin polarization of low energy secondary electrons generated in an SEM were suggested by Unguris et al. (1982): 1) high spatial resolution is possible with a suitable SEM, 2) the polarization signal is proportional to the magnetization under the electron beam, and 3) the contrast should be high and independent of topographic contrast. The first such measurements were made by Koike and Hayakawa (1984a, 1984b) who initially combined a 10 μm electron beam from a scanning electron gun with a high energy Mott spin analyzer to produce SEMPA images. They demonstrated that a high contrast independent of topographic contrast could indeed be achieved. Subsequently Koike et al. (1985 a,b,c), and Koike and Haykawa (1985), using much improved electron guns to achieve higher spatial resolution, have demonstrated many advantages of the SEMPA technique in a research program which parallels ours at NBS (Unguris et al., 1985, 1986b). The main difference between the two efforts is instrumental. Instead of a high energy Mott spin analyzer, at NBS we have added specially designed compact low energy spin analyzers to a commercial field emission scanning electron microscope. The rest of this paper will be devoted to the NBS development of SEMPA and some illustrative results to demonstrate its capabilities. A companion paper in these proceedings (by Koike et al., 1987) describes the work of that group.

Principle of SEMPA

The principle of SEMPA is illustrated schematically in Fig. 1. High energy electrons in the SEM are shown incident on a domain in the specimen. Within each domain there is a magnetization or magnetic moment per unit volume $\vec{M}$ along a particular direction. In 3d ferromagnets where the orbital magnetic moment is quenched, the magnetization is proportional to the net electron spin density $n_\uparrow - n_\downarrow$, where $n_\uparrow (n_\downarrow)$ are the number of spins per unit volume parallel (antiparallel) to the particular direction. We have for the magnetization:

$$M = -\mu_B (n_\downarrow - n_\uparrow) \qquad (1)$$

where the minus sign is because the electron spin $\vec{s}$ (units of $\hbar/2$) and electron spin magnetic moment $\vec{\mu}$ (units of Bohr magneton, $1\,\mu_B = 0.927\times10^{-23}$ J/T) point in opposite directions, $\vec{\mu} = -\mu_B\vec{s}$.

The secondary electrons generated in the SEM are collected and their polarization is measured. The polarization, like the magnetization, is a vector

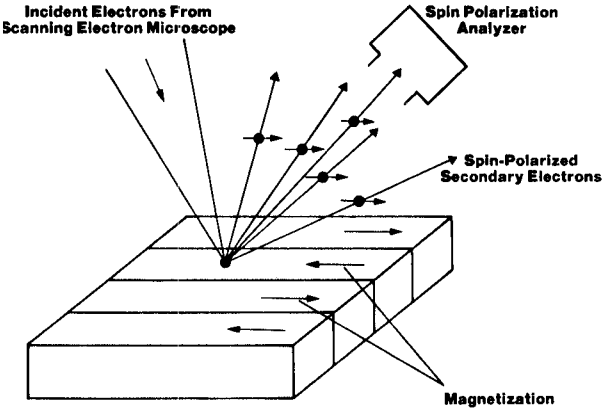

Figure 1. Principles of scanning electron microscopy with polarization analysis (SEMPA).

quantity. For a pure spin state the polarization is defined as the expectation value of the Pauli spin operator σ

$$\vec{P} = \langle \vec{\sigma} \rangle . \qquad (2)$$

Electron beams consist of an ensemble of different spin states and the polarization is defined in terms of the density matrix ρ as:

$$\vec{P} = \mathrm{tr}(\rho\vec{\sigma})/\mathrm{tr}\rho, \qquad (3)$$

where tr denotes the trace. From the point of view of SEMPA, it is sufficient to consider each component of the polarization separately and use the conceptually simpler definition of the polarization, for example, in the z direction,

$$P_z = \frac{N\uparrow - N\downarrow}{N\uparrow + N\downarrow} \qquad (4)$$

where $N_\uparrow (N_\downarrow)$ are the number of electrons with spins parallel (antiparallel) to the z direction. The polarization may have values $-1 \leq P \leq 1$.

The large low energy secondary electron peak is the result of exciting many electron hole pairs in the valence band. The spin polarization for a representative sample of the valence band electrons can be estimated from:

$$P = n_B/n \qquad (5)$$

where n is the total number of valence electrons per atom and n_B, the Bohr magneton number/atom, is just the difference in the number of up and down valence electron spins per atom. The following table shows the spin polarization to be expected on the basis of these arguments for Fe, Co, and Ni.

Table 1. Predicted Polarization

	n_B	n	P
Fe	2.22	8	0.28
Co	1.72	9	0.19
Ni	0.54	10	0.054

In fact, there is evidence, as mentioned in the Introduction, for an enhancement of the low energy spin polarization. A spin dependent mean free path has been suggested to explain the observed enhancement (Glazer and Tosatti, 1984; Penn, et al., 1985). The content of the magnetic microstructure image is not changed as long as the enhancement of the polarization is not position dependent but remains constant as the SEM beam rasters over the specimen. The same applies to a decrease in the polarization, but there is no evidence for this to date.

We note that the contrast in such a polarization image of magnetic domains is expected to be quite high. Using the estimates from Table 1, in an iron specimen, for example, the polarization goes from +28% in one domain to -28% in a neighboring domain oriented in the opposite direction. When the enhancement of the polarization is taken into account the contrast can be even higher.

In determining the polarization, the difference in the number of electrons with spin of one orientation and of electrons with spin of the opposite orientation is measured, i.e., the numerator in Eq. (4). But also, the total number of secondary electrons arriving at the detector is measured, i.e., the denominator in Eq. (4). This latter signal gives the topographical image in a conventional SEM micrograph. The spin difference of the numerator is normalized by the total current. Thus the measured polarization is independent of the topography, unless, of course, the topography actually affects the magnetic microstructure. This is an important advantage of SEMPA over most magnetic contrast techniques: the topographical and magnetic images are measured simultaneously but independently and do not interfere with each other.

The resolution which can be obtained in a magnetic image with SEMPA is the same as that of a conventional topographical image and ultimately depends on the size of the SEM electron beam. We have demonstrated 50nm resolution (cf. Fig. 8(d)) in SEMPA images and believe we will be able to go below 10 nm when the SEM works to specifications.

The secondary electrons come from depths of a few nanometers. Unlike the topographic image which is not disturbed by a uniform layer of contaminant on the surface, the magnetic image is very sensitive to contamination since the magnetic information is contained in the polarization of the secondary electrons which come from the outer atomic layers. The magnetic image is lost if there are nonmagnetic contaminant layers on the surface. For this reason, specimens to be measured by SEMPA must be cleaned by traditional surface science methods in ultra high vacuum.

The Instrument

Scanning Electron Microscope

An ultra high vacuum SEM is required for SEMPA. A schematic of our SEMPA system, with the size of the spin analyzers greatly exaggerated, is shown in Fig. 2. We use a VG HB50A modified to include a magnetic gun lens. Typical pressures during operation are $2\text{-}5\times10^{-10}$ Torr. Typical operating conditions are 1-5 nA beam current, 60 nm beam diameter, at 20 keV beam energy. This beam energy provides a good compromise between secondary electron production and resolution.

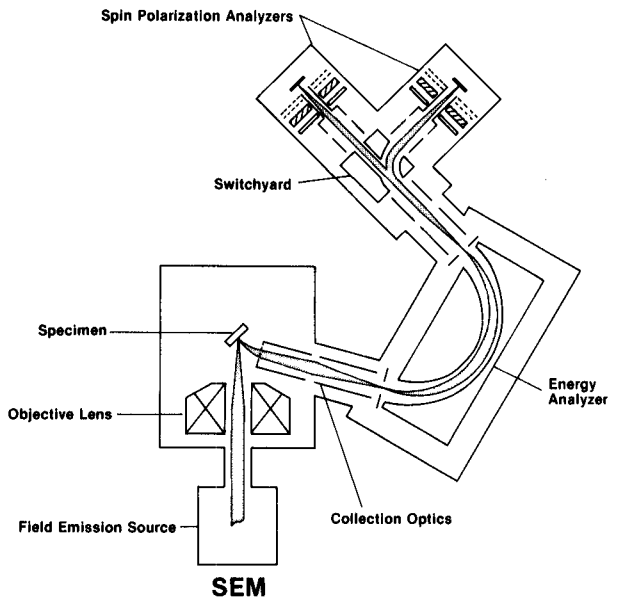

Figure 2. Schematic of the SEMPA apparatus (not to scale) showing two orthogonal spin analysers to measure all three components of the electron spin polarization.

The working distance is 25 mm. A distance of approximately this amount is useful to allow room for extraction electron optics to be inserted near the specimen. The maximum magnetic field of the objective lens at the specimen is 4 Oe. Higher fields could be detrimental in two ways: 1) the field could change the magnetic microstructure in soft (low coercivity) ferromagnets, and 2) the field could affect the trajectories and even the spin polarization of the secondary electrons. We have found that, if necessary, a simple bucking coil can be used to reduce the field at the specimen and in the region to the entrance of the collection optics to less than +0.5 Oe.

Collection and Transport Electron Optics

In the ideal situation, it would be convenient to have the axis of the collection optics perpendicular to the specimen surface and accelerate the secondary electrons in a parallel plate geometry. This is not the case for our instrument because of the constraints of the existing vacuum chamber. We accelerate the secondaries in a nonparallel geometry to a grid in front of cylindrical lens elements so placed that the secondary beam is on axis. The secondary electrons are accelerated to 1500 eV and transported to the spin analyzers without changing the direction of electron spin. An existing Auger energy analyzer is operated at a pass energy of 1500 eV and selects the 0-15 eV secondary electrons. Such an energy analyzer is not required for SEMPA as sufficient energy selection can be achieved without it.

Each spin analyzer determines two orthogonal transverse components of the electron beam polarization. To determine the component of polarization normal to the specimen surface in Fig. 2, a second analyzer is place 90° to the first. The electron beam can be diverted to that analyzer in the "switchyard" consisting of an electrostatic deflector which changes the direction of the electron beam but not of the spin. A set of electron optics at the front of each spin analyzer changes the beam energy and focuses it onto the analyzer target.

Spin Polarization Analyzer

Many factors are important in considering a spin analyzer for a particular application. These include the operating energy, size, vacuum compatibility, electron optical acceptance, allowable energy spread, and efficiency. The statistical uncertainty ΔP in a measurement of the polarization of an electron beam is:

$$\Delta P = \sqrt{\frac{1}{NS^2}} \qquad (6)$$

where N is the number of scattered electrons and S is the analyzing power (basically the asymmetry in the scattering due to the spin polarization). Thus the efficiency not only depends on the ratio of scattered to incident electrons, $N/N_0 = I/I_0$, expressed in terms of the number of electrons or the electron current, but also on the analyzing power S. To compare different analyzers the figure of merit, S^2I/I_0, is used keeping in mind that the analyzer must also be able to accept the energy-area-solid angle product of the beam to be measured.

In other polarization studies to date, the Mott analyzer has traditionally been the most widely used. It is based on the spin-orbit induced asymmetry in the scattering of high energy (of order 100 keV) electrons from a thin Au foil (Kessler, 1985). Although the electron optical acceptance is excellent, and the figure of merit of an optimized Mott analyzer is as good as can be obtained otherwise, the high voltages make such an analyzer large, heavy, and not readily added to an SEM.

An efficient, low energy, compact spin analyzer based on polarized low energy electron diffraction (PLEED) has been described by Kirschner (1985). This spin analyzer is most suitable for measuring electron beams with energy spread less than 5 eV and angular spread less than 2°. For the measurement of secondary electrons this means a necessary loss of some signal. Moreover, the tungsten crystal target must be atomically clean, requiring flashing to ~2500K approximately each 15-30 min. (Kirschner, 1985).

We have developed a new spin analyzer which we believe is especially suited for SEMPA. It is based on low energy diffuse scattering from a high-Z target. It is compact (fist-sized), as efficient as the best high energy Mott analyzers, employs a stable (over weeks in UHV) scattering target, and has greatly relaxed constraints on the energy spread and angular spread of the electron beam. Thus it overcomes the drawbacks of previously available spin analyzers.

A schematic of the analyzer is shown in Fig. 3. The beam is incident at 150 eV on an evaporated Au film target. The weakness of the diffuse scattering is compensated by collection over a large solid angle. The crucial point is that the analyzing power remains substantial for electrons scattered over a large solid angle such that a figure of merit in excess of 10^{-4} is achieved. The low energy secondary electrons from the Au target are retarded at grid G2. The electron signal is multiplied at a chevron channel plate assembly and collected on a four-sector anode.

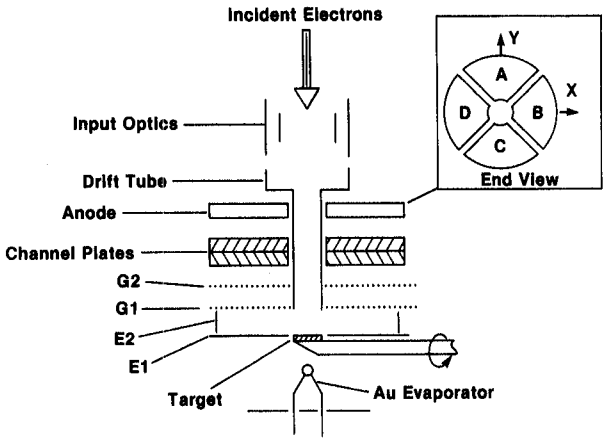

Figure 3. Schematic of the low-energy diffuse scattering spin analyzer. The inset shows the view of the anode seen by electrons emerging from the channel plate.

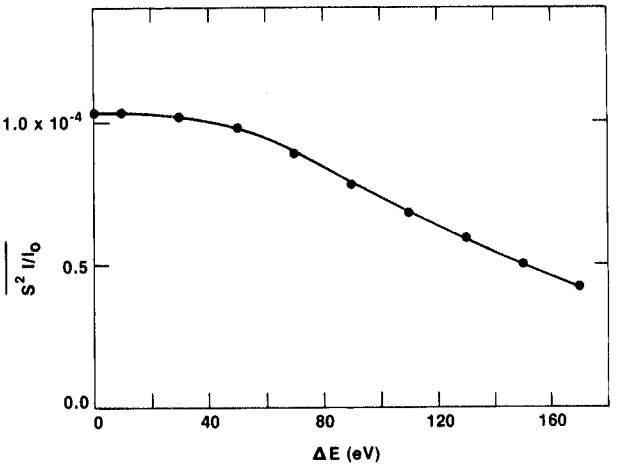

Figure 4. The average figure of merit $\overline{S^2 I/I_0}$ of the spin analyzer for incident electron beams with varying energy spread ΔE.

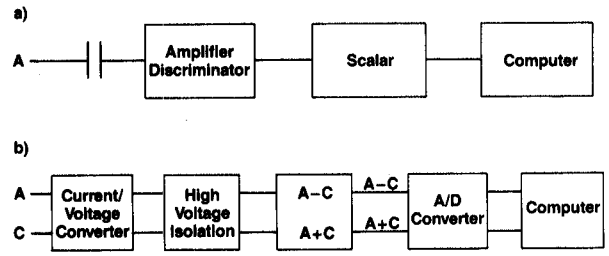

Figure 5. (a) Block diagram for data acquisition from each quadrant in the pulse counting mode. (b) Block diagram for analog data acquisition from two opposing quadrants.

The difference in the scattered currents I_A and I_C to quadrants A and C give the x component of polarization:

$$P_x = \frac{1}{S}\frac{I_C - I_A}{I_C + I_A} \qquad (7)$$

where the analyzing power S = 0.107. Complete details of this spin analyzer have been given by Unguris et al. (1986a). One interesting feature shown in Fig. 4 is the average figure of merit as a function of the energy spread of the incident electron beam. Clearly it is possible to measure a 20 eV energy spread of low energy secondary electrons from the specimen in the SEM without degradation of performance.

Data Acquisition

Two orthogonal spin analyzers, with a total of four identical polarization signal channels, are used to measure all three components of the electron spin polarization, one of them redundantly. A polarization channel has two currents one from each of two opposing quadrants. We have measured these currents in both the pulse counting and analog mode as shown in block diagram form in Figs. 5(a) and (b), respectively.

In the pulse counting mode, the anode sector which is at high voltage is isolated by a capacitor which passes the pulses to an amplifier/discriminator and then to a scaler which is read by the computer. The same holds for the opposite quadrant of the anode. The computer calculates the polarization and intensity at each position and plots and stores this information. In the first tests of the system, the incident SEM beam current at the specimen had to be reduced to 3×10^{-12}A to avoid count rates which would be excessive for the channel plates.

In order to take advantage of higher SEM beam currents the analog detection system of Fig. 5(b) is used. The currents at the high voltage anode are brought to near ground potential after passing through a current to voltage amplifier. The difference and sum of the signals from opposing quadrants is taken with analog circuitry and passed through a filter and the analog-to-digital converter to the computer which plots and stores the information.

It is of interest to calculate the threshold SEM beam current required for an image with a specified time per pixel or, alternatively, given the SEM beam current, the minimum time required to obtain an image. This involves calculating the minimum signal to noise to observe a given contrast in a polarization image which can be accomplished in a way similar to the calculation for an SEM intensity image (Newbury 1975). Consider the situation shown in Fig. 1 with the polarization axis of the spin analyzer along the magnetization direction. Moreover, consider the electrons to only one quadrant of the anode designated $N\uparrow$ coming from one domain and $N\downarrow$ coming from the neighboring domain. As the SEM beam scans perpendicular to the domain walls, the signal will appear as in Fig. 6. The number of electrons to the quadrant for the beam positioned on each of the two oppositely oriented domains is:

$$N_\uparrow = \bar{N}\,(1+SP) \qquad (8a)$$

$$N_\downarrow = \bar{N}\,(1-SP) \qquad (8b)$$

where S is the analyzing power, P is the beam polarization, and $\bar{N}$ is the average number of counts in the quadrant. The difference between the two signal levels is $N\uparrow - N\downarrow = 2SP\bar{N}$. The contrast C, which

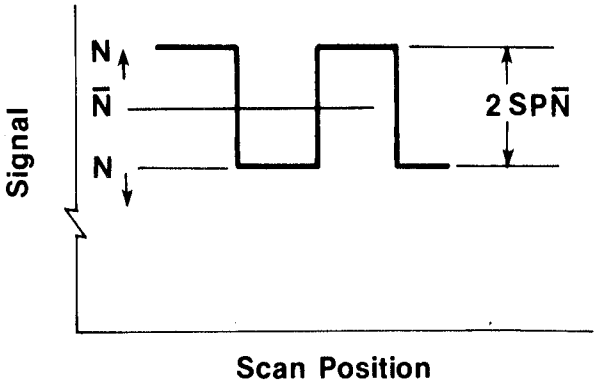

Figure 6. The number of electrons to one quadrant as the SEM beam is scanned across the domains as in Fig. 1.

is defined as the ratio of this difference to the average signal level, in this case $\bar{N}$, is just C=2SP.

The signal change must be greater than five times the noise for the eye to detect a change, and the noise is estimated at $2\sqrt{\bar{N}}$ instead of $\sqrt{\bar{N}}$ to account for random fluctuations in secondary production (Newbury, 1975). This leads to the inequality, $N_{\uparrow} - N_{\downarrow} > 10\sqrt{2\bar{N}}$, from which we have the criteria for the minimum number of counts for a given contrast:

$$\bar{N} > \frac{50}{P^2S^2} \qquad (9)$$

Alternatively, this condition can be restated in terms of the minimum current that needs to appear at the spin analyzer. This threshold current is,

$$I_{th} > \frac{(50/P^2S^2) \times 1.6 \times 10^{-19}}{t_p} \qquad (10)$$

where t_p is the time spent measuring a single picture element, i.e., pixel.

The threshold current is related to the SEM beam current by:

$$I_{th} = 1/2\ (N/N_o)\ T\ Y\ I_{SEM} \qquad (11)$$

where the factor of 1/2 arises because only two of the four quadrants are used to measure one polarization component, $N/N_o \approx 0.01$ is the scattering efficiency at the Au target, T=0.5 is the transmission of the electron optics, and Y=0.2 the secondary yield at 20 keV beam energy. Thus for our system:

$$I_{SEM} = 2\times10^3\ I_{th}.$$

For a SEM beam current of 1nA, and an iron specimen with P(Fe)=0.28 from Table 1, and S=0.107, for our spin analyzer, the pixel time is approximately 18 msec. At present we scan 128x96 pixel images in about 15 min. or approximately 70 msec/pixel. We are presently not yet at the shot noise limit due to noise in the prototype electronics and possibly additional channel plate noise beyond the factor of two assumed above. Some time is also unnecessarily lost in the computer operations. We are working on improving the data acquisition electronics with the potential of increasing our speed of data acquisition.

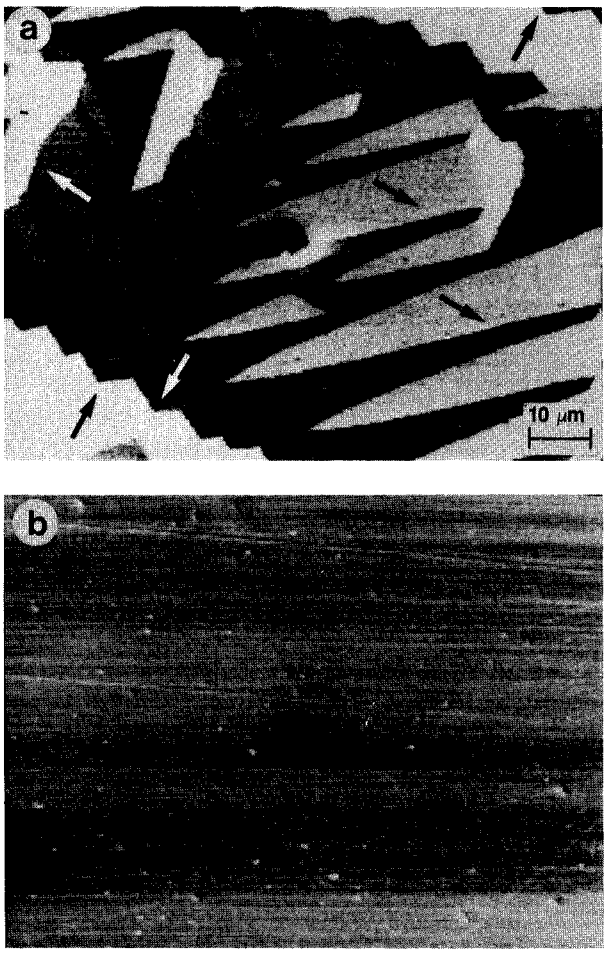

Figure 7. Polarization image (a) and intensity image (b) of Fe-3%Si single crystal. The gray levels give the four different magnetization directions in the domains as marked by the arrows.

Results

In this section we select a few results from various studies we have made of numerous materials to illustrate the following special features of SEMPA: 1) SEMPA can yield all three component of the polarization thereby providing an image of the vector magnetization. 2) The contrast and signal are large. 3) The magnetic image is independent of surface topography unless the topography is actually affecting the magnetic microstructure. 4) High spatial resolution can be obtained. 5) The technique is surface sensitive.

The studies which have been selected to illustrate these features involved Fe-3% Si single crystals, permalloy thin films for recording heads, a CoNi recording media, and ferromagnetic metglasses of varying magnetostriction. We present the micrographs of each material in turn. Each

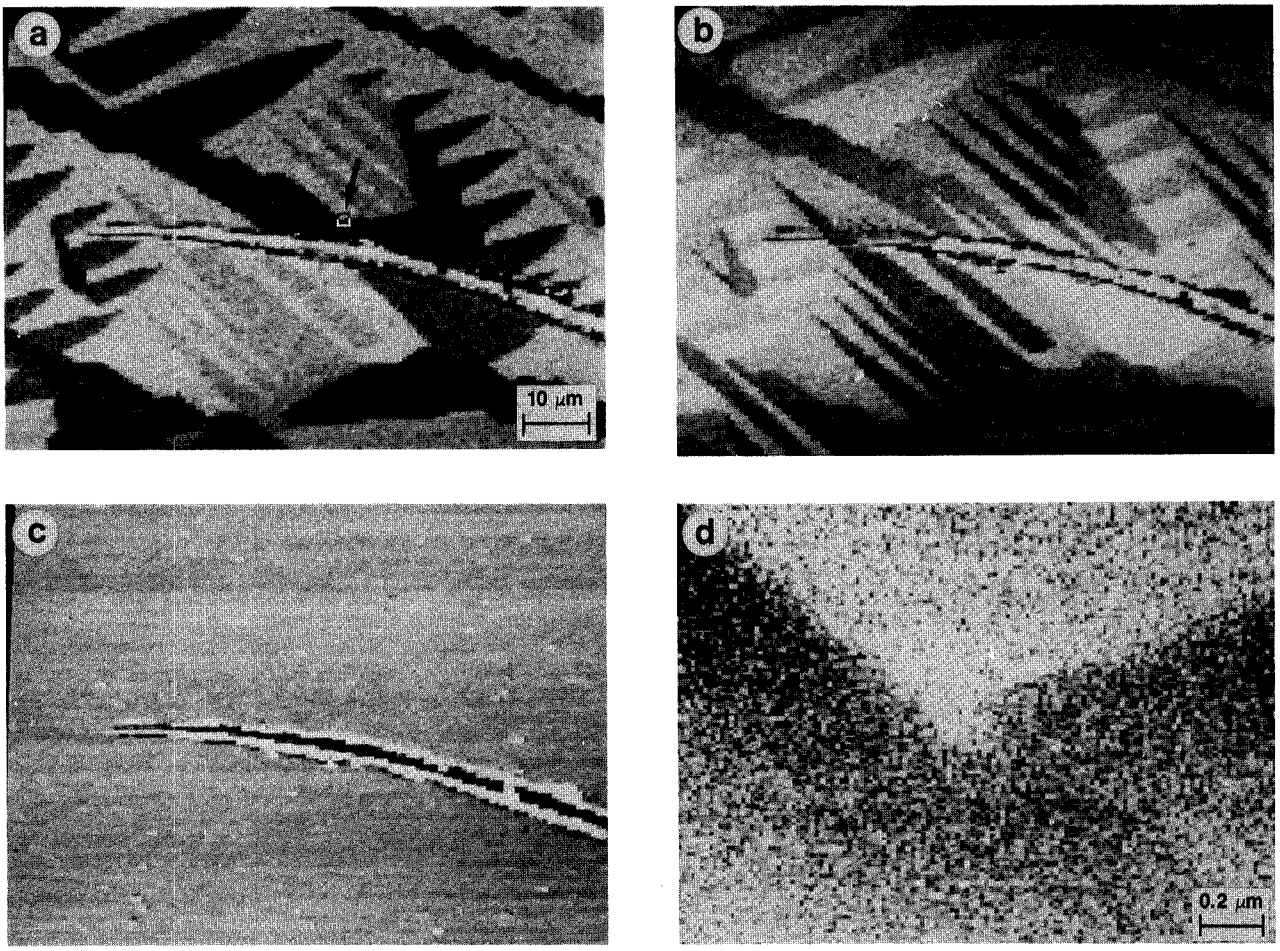

Figure 8. Images (a) and (b) from measuring two (orthogonal) in-plane components of the polarization is an Fe-3%Si single crystal. (c) The intensity image of the same area. (d) 50 x magnification of the region marked in (a).

micrograph illustrates one or more of the salient features of the SEMPA technique which will be the emphasis of this discussion rather than the information about magnetism, which will be discussed elsewhere.

Iron-silicon Single Crystal

The Fe-3%Si single crystal specimens were prepared by mechanical polishing. A regular domain pattern is observed when the crystal is oriented such that the surface contains the easy axes of magnetization, [100] and [010] for a (001) surface. When the crystal is cut a few degrees off an easy axis, very striking irregular domain patterns occur, including the so called "fir-tree" pattern (Williams et al., 1949). Figs. 7-9 are from a Fe-3%Si crystal cut approximately 4° off the [100] axis. The surfaces were cleaned by cycles of Ar ion bombardment followed by annealing to 600°C.

Fig. 7 shows a polarization image (a) and intensity image (b) from such an Fe-Si crystal. The polarization image is that obtained from a measurement of one component of the polarization. Four distinct gray levels are observed and correspond to domain magnetization as indicated by the arrows. The spin analyzer polarization axis is rotated 28° with respect to the [100] easy axis of magnetization. Thus, for the magnetization along the [100] axis, a polarization $P' = +P\cos(28^\circ) = +0.9P$ is measured, where $P \simeq 22\%$ is the value along an easy axis. For domains with magnetization along a [010] direction the measured polarization is $P' = +P\cos(62^\circ) = 0.56P$. The zig-zag domain wall running across the lower left corner of Fig. 7(a) is a common means to minimize the energy in such microstructure as discussed by Chikazumi and Suzuki (1955). The disturbance in the domain pattern near the center of Fig. 7(a) can be seen to arise from the defect in the crystal apparent in the intensity image.

Each spin analyzer measures two components of the polarization along two orthogonal directions. An example of this is seen in Figs. 8(a) and (b). These images, like Fig. 7, are taken at relatively low magnification to display the interesting domain patterns. Figs. 8(a) and (b) are seen to be complementary as expected. The light and dark regions of Fig. 8 (a) show up as intermediate gray levels in the orthogonal polarization image, Fig. 8(b), and vice versa. There is a large scratch across the crystal as seen in Fig. 8(c). The small region near the center of Fig. 8(a) (marked) is shown magnified

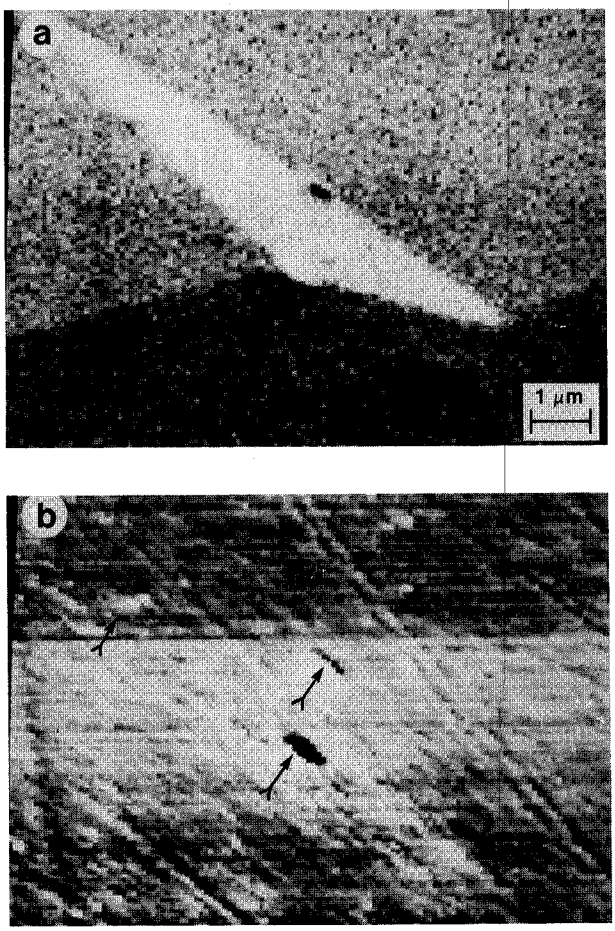

Figure 9. High resolution polarization (a) and intensity (b) images show how the walls separating the three domains in (a) are pinned by the three defects observed in (b).

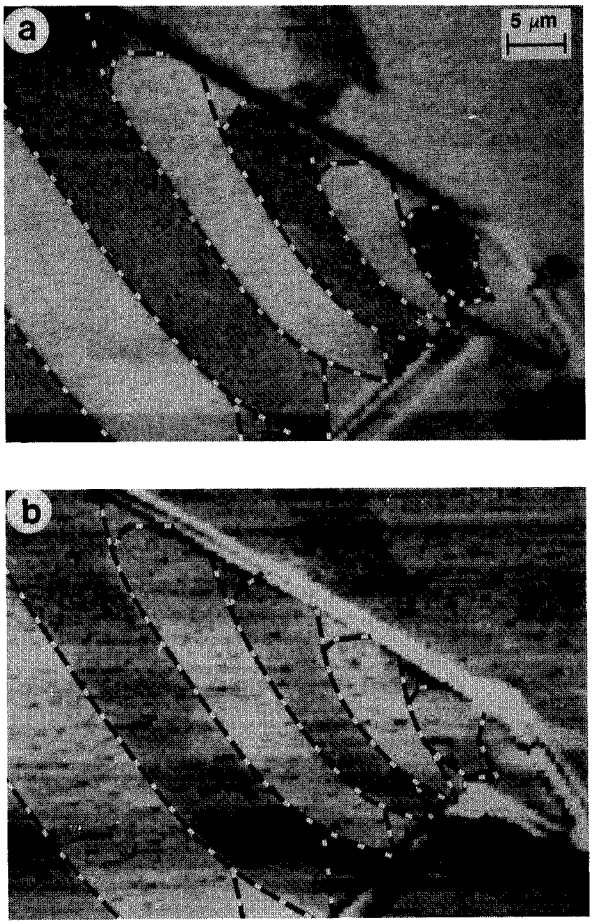

Figure 10. A polarization image of one of the layers of a permalloy thin film recording head (a) and the orthogonal polarization image (b).

fifty times in Fig. 8(d). Submicrometer resolution is clearly achieved.

In the high magnification image of Fig. 9(a) an interesting dagger like domain structure was observed on an Fe-3%Si crystal. There are three dominant gray levels indicating three magnetization directions in three different domains. This example shows a striking correlation between the domain boundaries and the three defects observed in the intensity image, Fig. 9(b). Each defect occurs at a domain wall and, in fact, is apparently pinning the position of the domain wall. This action by defects is one of the major sources of magnetic coercivity. The coercive field, i.e., that opposing field required to reduce the magnetization of a saturated magnet to zero, is a property that varies by many orders of magnitude. The ability of SEMPA to establish the effect of physical structure on magnetic structure is expected to be very useful in investigations of the origins of coercivity.

Permalloy Thin Film Magnetic Recording Head

Permalloy is a high permeability iron-nickel alloy usually containing 50 to 80% Ni. This polycrystalline disordered alloy has many applications in devices and machines. It is magnetically soft, i.e., easy to magnetize and demagnetize, as opposed to a magnetically hard material that would be used for a permanent magnet.

A thin film permalloy head consists of a sandwich of two permalloy films separated by a spacer and a Cu energizing coil. This technology has made it possible to decrease the gap at the pole tips to achieve higher recording density. The high frequency response of a thin film permalloy head is better, for example, than that of a ferrite head. Two orthogonal polarization images of one of the permalloy layers of a thin film head are shown in Figs. 10(a) and (b). The advantage of SEMPA, in this case, is the ability to observe the two polarization images simultaneously which enables one to readily identify the closure domains at the edges of the thin film structure (highlighted in Fig. 10). The closure domains have a different frequency response than the other domains and thus reduce the speed with which the head can read or write. The high resolution of SEMPA is advantageous for investigating the pole tip region where optical

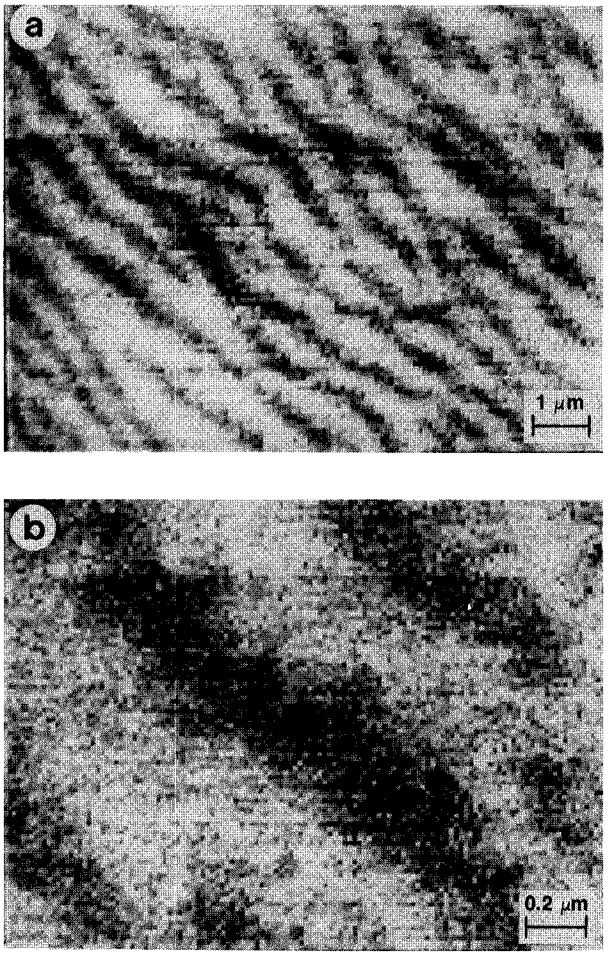

Figure 11. Co-Ni recording media in demagnetized state to show fine domain structure similar to written bits (a). A 5 x magnification of a region of (a) showing the irregularity of the domain walls.

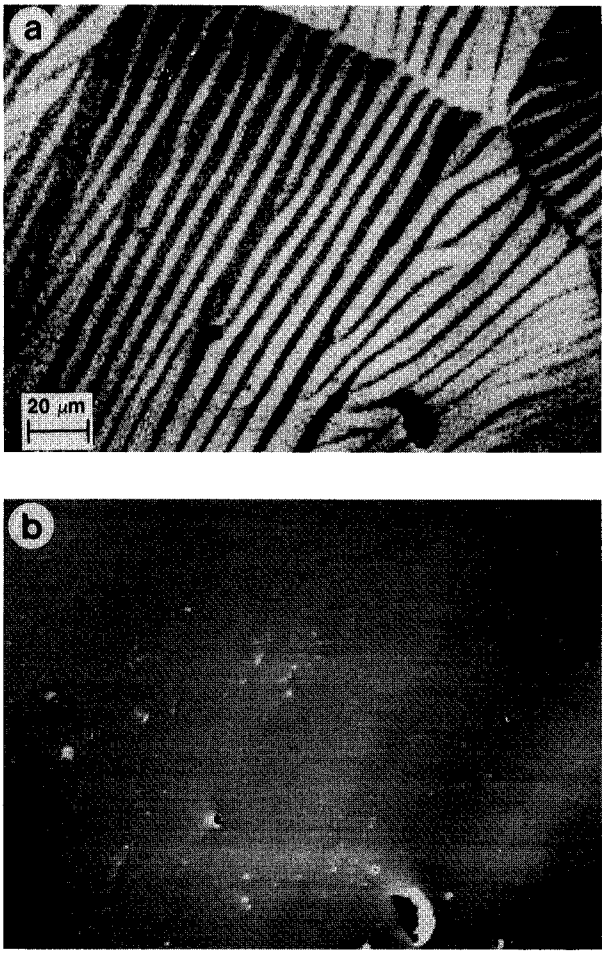

Figure 12. Fine domain structure of an Fe-based metglass shown in (a) with corresponding intensity image in (b).

resolution fails. Small domains in the pole tip region are a source of noise.

Co-Ni Recording Media

With the aim of obtaining higher density information storage, much effort is being invested in finding a magnetic recording medium on which small, sharply defined bits can be written. One of the prototype media is an 80%Co-20%Ni film grown so as to produce canted columns in order to increase the sharpness of the magnetic boundaries known as edge acuity. Frequently, domain boundaries take a zig-zag form to reduce the overall energy. Since the signal from a magnetic record comes when there is a transition from one magnetization direction to another, a zig-zag wall manifests itself in decreased sharpness of the transition and hence noise. The recording industry is eager to observe the boundaries of magnetic regions far smaller than can be observed optically.

Fig. 11 shows our SEMPA images from a Co-Ni film on a Si substrate. This specimen did not have magnetic bits written on it. Small magnetic regions which simulate a written record were obtained by demagnetizing the film. In Fig. 11(a) the light and dark striped pattern corresponds to magnetization reversals of 180°. The magnetization is perpendicular to the length of the stripes. The high resolution and contrast of SEMPA allows one to examine in detail the edge acuity in the magnified image shown in Fig. 11(b).

Ferromagnetic Metglass

Amorphous ferromagnetic glasses can have many useful characteristics such as low coercivity and losses, and high permeability and high magnetostrictive coupling. In an effort to understand possible origins of differences in the magnetostrictive coupling properties of some Fe-based ferromagnetic glasses, a survey of the domain structure was made yielding polarization and intensity images as shown in Figs. 12(a) and (b).

Instead of the broad (∿100 μm wide) regular domains expected for this metglass ribbon annealed in a transverse magnetic field, in certain areas we observe a very fine, complex domain pattern as shown in Fig. 12(a). Such patterns are due to closure domains at the surface resulting from there being an easy axis perpendicular to the surface induced by stress. In fact, it is possible to study stresses in the specimens by observing domain patterns (Livingston, 1985). Figure 12(a) exhibits better contrast and definition than can be obtained

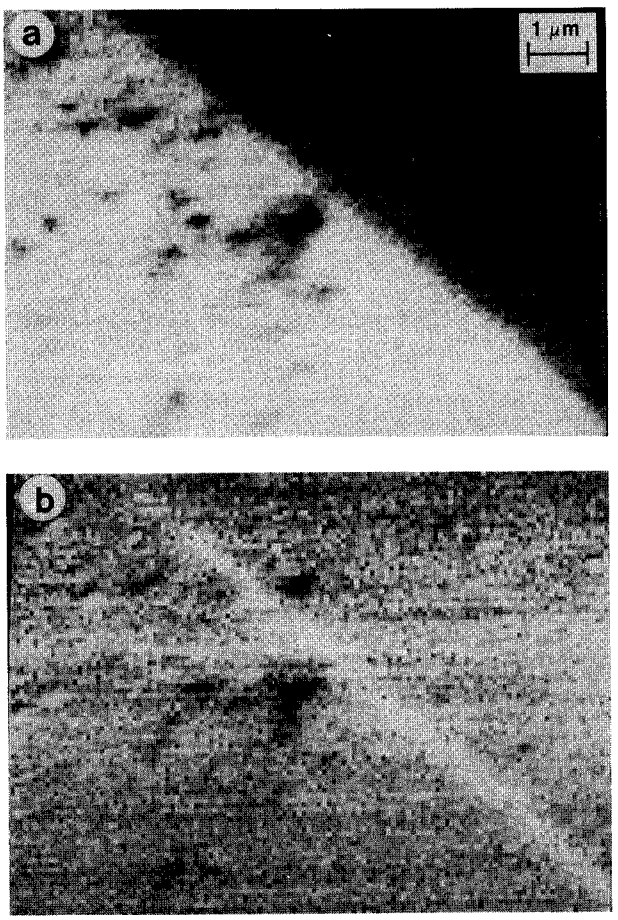

Figure 13. Image of magnetization along the line of the domain wall (a) and perpendicular to it (b). The approximately 0.5 μm wall is clearly observed in (b) indicating a Neél like wall in the surface region.

by domain imaging with the Bitter technique or magneto-optic Kerr effect. The intensity image shows the topography of the ribbon which reflects the copper wheel on which it was quenched. Note the broad vertical bands, suggesting a wavy surface on this part of the wheel. The two large point-like defects are seen to influence the course of the domains shown in the polarization image.

A higher magnification image of a domain wall in a metglass without stress defects is shown in Fig. 13. Two orthogonal polarization components are shown in Figs. 13 (a) and (b). In Fig. 13(a) there is a light region on the left and a dark region on the right. The direction of magnetization is parallel to the boundary, in one direction on one side and in the opposite direction on the other. For a simple Bloch wall we expect an out of plane rotation of the spins as the spins rotate 180° across the domain wall. Instead, we find in Fig. 13(b) that in the image of the other in-plane polarization component, the wall region of about 0.5 μm width is well defined. This can only be explained by an in-plane component of the magnetization perpendicular to the wall, that is a Neél type wall at least in the surface region probed by the secondary electrons. Thus, the surface sensitivity allows us to observe directly an in-plane spin rotation as predicted by Hubert (1971), while in the interior of the ribbon the change of spin direction is expected to be that of a Bloch wall.

Conclusions and Future Prospects

The five salient features of SEMPA listed at the beginning of our discussion of results have been illustrated, but have just begun to be applied to the many problems whose investigation could benefit from those advantages. The applications are so numerous in high density magnetic storage that we expect SEMPA to be a routine tool in laboratories concerned with the development of recording media and devices. Both soft and hard magnetic materials will benefit from SEMPA studies. In particular the origin of the high coercivity in such new materials as $Nd_2Fe_{14}B$ will be studied. The combination of SEMPA with scanning Auger spectroscopy will allow an investigation of whether a defect pinning a domain wall is simply structural or is compositional, such as a precipitate or segregate to a grain boundary. Such a combination, which is natural since both scanning Auger and SEMPA operate in ultrahigh vacuum, will be powerful indeed.

As data acquisition is optimized to operate near the shot noise limit, it should be possible with an SEM and with a properly operating field emission gun to achieve a very high spatial resolution of $\lesssim$5 nm. There are many fundamental questions such as the details of spin variation in a domain wall, or around Bloch lines and Neel lines that will be susceptible to investigation by SEMPA. Of interest also is the influence of size effects when a fabricated structure such as a memory element has dimensions comparable to wall widths. The influence of dimensionality as in a 2-d film poses many questions. Because SEMPA is surface sensitive, even very thin films can be investigated with SEMPA. Recent calculations of an idealized single layer Fe film (Gay and Richter, 1986) found a large anisotropy perpendicular to the film plane. In a real system the perpendicular magnetization may break up into small domains which should be readily observable by SEMPA but impossible to see with spatially averaging techniques.

Although still in its infancy, SEMPA can be expected to have a bright future and a large impact in the many areas where investigation of magnetic microstructure is important.

Acknowledgments

Several of the figures used here to demonstrate the features of SEMPA are a result of a very productive collaboration with a number of institutions. We wish to thank Control Data Corporation for the thin film head specimen imaged in Fig. 10, Eastman Kodak Co. for the Co-Ni media imaged in Fig. 11, and the Magnetism Group of the Naval Surface Weapons Center for providing and magnetically preparing the amorphous ferromagnetic samples imaged in Figs. 12 and 13. We wish to acknowledge the collaboration of Dr. Claudio Aroca of the Universidad Complutense, Madrid, Spain, in the study of the magnetic metglass specimens and the U.S.-Spain Committee for Scientific and Technological Cooperation which made the collaboration possible. The development of the SEMPA technique and the measurements reported

here have been supported in part by the Office of Naval Research. Identification of commercial equipment in order to more clearly describe our apparatus does not imply recommendation or endorsement by the National Bureau of Standards, nor does it imply that the equipment identified is necessarily the best available for the purpose.

References

Bitter F. (1931). On inhomogeneities in the magnetization of ferromagnetic materials. Phys. Rev. 38, 1903-1908.

Celotta RJ, Pierce DT. (1986). Polarized electron probes of magnetic surfaces. Science 234, 333-340.

Celotta RJ, Pierce DT. (1982). Possibilities for the use of electron spin polarization in scanning electron microscopy, in: Microbeam Analysis-1982, K.F.J. Heinrich (ed), San Francisco Press, 469-470.

Chapman JN, Morrison GR. (1983). Quantitative determination of magnetization distributions in domains and domain walls by scanning transmission electron microscopy. J. Mag. Mag. Matls. 35, 254-260.

Chikazumi S, Suzuki K. (1955). On the maze domain silicon-iron crystal (I). J. Phys. Soc. Japan 10, 523-534.

Chrobok G, Hofmann M. (1976). Electron spin polarization of secondary electrons ejected from magnetized europium oxide. Phys. Lett. 57A, 257-258.

DiStefano TH. (1978). Technology for detecting small magnetic domains and beam addressed memory therewith. IBM Tech. Discl. Bull 20, 4212-4215.

Gay JG, Richter R. (1986). Spin anisotropy of ferromagnetic films. Phys. Rev. Lett. 56, 2728-2731.

Glazer J, Tosatti E. (1984). Theory of spin-flip excitations across the ferromagnetic Stoner gap in electron energy loss. Solid State Commun. 52, 905-908.

Hopster H, Raue R, Kisker E, Guntherodt G, Campagna M. (1983). Evidence for spin dependent electron-hole-pair excitations in spin polarized secondary electron emission from Ni(110). Phys. Rev. Lett. 50, 70-73.

Hubert A. (1971). Blochwände in dicken magnetischen Schichten. Z. Angew. Phys. 32, 58-63.

Jakubovics JP. (1973). Lorentz microscopy and applications (TEM and SEM). in: Electron Microscopy in Materials Science Part IV, E. Ruedl, U. Valdre (eds), Commission of the European Communities, Brussels, 1305-1403.

Kessler J. (1985). Polarized Electrons, Springer-Verlag, Berlin, 230-244.

Kirschner J. (1984). On the role of the electron spin in scanning electron microscopy. Scanning Electron Microsc. 1984;III:1179-1185.

Kirschner J. (1985). Polarized Electrons at Surfaces, Springer-Verlag, Berlin, 61-71.

Kisker E, Gudat W, Schröder K. (1982). Observation of high spin polarization of secondary electrons from single crystal Fe and Co. Solid State Commun. 44, 591-595.

Koike K, Hayakawa K. (1984a). Scanning electron microscope observation of magnetic domains using spin polarized secondary electrons. Jpn. J. Appl. Phys. 23, L187-L188.

Koike K, Hayakawa K. (1984b). Observation of magnetic domains with spin-polarized secondary electrons. Appl. Phys. Lett. 45, 585-586.

Koike K, Hayakawa K. (1985). Domain observation with spin-polarized secondary electrons. J. Appl. Phys. 57, 4244-4248.

Koike K, Matsuyama H, Todokoro H, Hayakawa K (1985a). Spin-polarized scanning electron microscope for magnetic domain observation. Jpn. J. Appl. Phys. 24, L542-L544.

Koike K, Matsuyama H, Todokoro H, Hayakawa K. (1985b). Spin-polarized scanning electron microscopy. Jpn. J. Appl. Phys. 24, 1078-1081.

Koike K, Matsuyama H, Todokoro H, Hayakawa K. (1985c). High spatial resolution spin-polarized scanning electron microscope. Jpn. J. Appl. Phys. 24, L833-L834.

Koike K, Matsuyama H, Hayakawa K. (1987). Spin polarized scanning electron microscopy for micro-magnetic structure observation. In: Physical Aspects of Microscopic Characterization of Materials, J. Kirschner, et al., (eds.) Scanning Microscopy Supplement 1, Scanning Microscopy International, AMF O'Hare, IL, 241-253.

Livingston JD. (1985). Magnetic domain, anisotropies, and properties of amorphous metals. J. Appl. Phys. 57, 3555-3559.

Newbury DE. (1975). Image formation in the scanning electron microscope, In: Practical Scanning Electron Microscopy, JI Goldstein, H Yakowitz (Eds.) Plenum Press, New York, 95-148.

Newbury DE, Joy DE, Echlin P, Fiori CE, Goldstein JI. (1986). Advanced Scanning Electron Microscopy and X-ray Microanalysis, Plenum Press, New York, 147-179.

Penn DR, Apell SP, Girvin SM. (1985). Theory of spin polarized secondary electrons in transition metals. Phys. Rev. Lett. 57, 518-521.

Tonomura A. (1983). Observation of magnetic domain structure in thin ferromagnetic films by electron holography. J. Mag. Mag. Matls. 31-34, 963-969.

Unguris J, Pierce DT, Galejs A, Celotta RJ. (1982). Spin and energy analyzed secondary electron emission from a ferromagnet. Phys. Rev. Lett. 49, 72-76.

Unguris J, Hembree GG, Celotta RJ, Pierce DT. (1985). High resolution magnetic microstructure imaging using secondary electron spin polarization analysis in a scanning electron microscope. J. Microscopy 139, RP1-RP2.

Unguris J, Pierce DT, Celotta RJ. (1986a). Low-energy diffuse scattering electron-spin polarization analyzer. Rev. Sci. Instrum. 57, 1314-1323.

Unguris J, Hembree GG, Celotta RJ, Pierce DT. (1986b). Investigations of magnetic microstructures using scanning electron microscopy with spin polarization analysis. J. Mag. Mag. Matls. 54-57, 1629-1630.

Williams HJ, Bozorth RM, Shockley W. (1949). Magnetic domain patterns on single crystals of silicon iron. Phys. Rev. 75, 155-183.

Discussion with Reviewers

J. Chapman: The magnetic signal is proportional to the in-plane component of magnetic flux integrated along the electron trajectory and so includes many contributions from stray fields above or below the specimen - it does not stop at the specimen surface.

Authors: In transmission electron microscopy the magnetic signal is given by the change in the phase of the electron wave caused by the integrated effect of the in-plane magnetic induction either within or outside the specimen. In contrast, in SEMPA the spin-polarization of secondary electrons is measured which is directly proportional to the net electron spin density in the specimen and hence to the magnetization. The magnetization may be in-plane or normal to the surface. Magnetic fields outside the specimen affect the polarization only to the extent which they cause the electron magnetic moments to precess. To have such an effect the magnetic fields must be both macroscopic and transverse to the polarization. Fields due to microscopic domains fall off over dimensions of order the domain size and do not cause significant electron depolarization. Fields due to the SEM pole piece or applied fields to magnetize the specimen must be closely controlled to be sure that the integrated effect on the secondary electrons passing through such a field is not sufficient to cause significant precession of the electron magnetic moments in the beam.

J. Chapman: In Eq.(11), does T = 0.5 imply that one half of the emitted secondary electrons are collected? Further, does a value Y = 0.2 allow for the fact that only a restricted energy range of the secondary electrons is used to form the images?
Authors: The value Y = 0.2 is a typical secondary electron yield for a primary SEM beam energy of 20keV. The value T = 0.5 is the fraction of those electrons in the appropriate energy range which are transmitted by the electron optics to the Au scattering target of the spin analyzer.

J. Chapman: Figure 10 seems to show strong contrast effects outside as well as inside the head, particularly towards the top center of the figure. To what are these due?
Authors: This specimen is at an intermediate stage of magnetic recording head production. A permalloy film has been deposited on a Si chip and lines of permalloy have been etched away to define the head shape. Magnetic material remains outside the head structure and gives the image contrast in question.